Mon. Not. R. Astron. Soc. **000**, 000–000 (0000) Printed 3 October 2014 (MN LaTeX style file v2.2)

Type Ia Supernova Spectral Features in the Context of Their Host Galaxy Properties

Y.-C. Pan[1,2⋆], M. Sullivan[2], K. Maguire[3], A. Gal-Yam[4], I. M. Hook[1,5], D. A. Howell[6,7], P. E. Nugent[8,9], P. A. Mazzali[10,11,12]

[1] *Department of Physics (Astrophysics), University of Oxford, DWB, Keble Road, Oxford OX1 3RH, UK*
[2] *School of Physics and Astronomy, University of Southampton, Southampton, SO17 1BJ, UK*
[3] *European Southern Observatory (ESO), Karl-Schwarzschild-Str.2, 85748 Garching b. München, Germany*
[4] *Department of Particle Physics and Astrophysics, Weizmann Institute of Science, Rehovot 76100, Israel*
[5] *INAF Osservatorio Astronomico di Roma, via Frascati, 33, 00040 Monte Porzio Catone, Roma, Italy*
[6] *Las Cumbres Observatory Global Telescope Network, Goleta, CA 93117, USA*
[7] *Department of Physics, University of California, Santa Barbara, CA 93106-9530, USA*
[8] *Department of Astronomy, University of California, Berkeley, CA 94720-3411, USA*
[9] *Computational Cosmology Center, Lawrence Berkeley National Laboratory, 1 Cyclotron Road, Berkeley, CA 94720, USA*
[10] *Astrophysics Research Institute, Liverpool John Moores University, 146 Brownlow Hill, Liverpool L3 5RF, UK*
[11] *INAF – Osservatorio Astronomico, vicolo dellOsservatorio, 5, I-35122 Padova, Italy*
[12] *Max-Planck Institut fur Astrophysik, Karl-Schwarzschild-Str. 1, D-85748 Garching b. München, Germany*

3 October 2014

ABSTRACT

We analyse spectroscopic measurements of 122 type Ia supernovae (SNe Ia) with $z < 0.09$ discovered by the Palomar Transient Factory, focusing on the properties of the Si II λ6355 and Ca II 'near-infrared triplet' absorptions. We examine the velocities of the photospheric Si II λ6355, and the velocities and strengths of the photospheric and high-velocity Ca II, in the context of the stellar mass (M_{stellar}) and star-formation rate (SFR) of the SN host galaxies, as well as the position of the SN within its host. We find that SNe Ia with faster Si II λ6355 tend to explode in more massive galaxies, with the highest velocity events only occuring in galaxies with $M_{\mathrm{stellar}} > 3 \times 10^9\, M_{\odot}$. We also find some evidence that these highest velocity SNe Ia explode in the inner regions of their host galaxies, similar to the study of Wang et al. (2013), although the trend is not as significant in our data. We show that these trends are consistent with some SN Ia spectral models, if the host galaxy stellar mass is interpreted as a proxy for host galaxy metallicity. We study the strength of the high-velocity component of the Ca II near-IR absorption, and show that SNe Ia with stronger high-velocity components relative to photospheric components are hosted by galaxies with low M_{stellar}, blue colour, and a high sSFR. Such SNe are therefore likely to arise from the youngest progenitor systems. This argues against a pure orientation effect being responsible for high-velocity features in SN Ia spectra and, when combined with other studies, is consistent with a scenario where high-velocity features are related to an interaction between the SN ejecta and circumstellar medium (CSM) local to the SN.

Key words: supernovae: general – circumstellar matter – distance scale.

1 INTRODUCTION

Type Ia supernovae (SNe Ia) are exceptional stellar explosions. They are believed to be the result of the thermonuclear explosion of an accreting carbon-oxygen white dwarf star in a close binary system. Although recent observations have constrained the size of the primary star to be consistent with a compact object (Nugent et al. 2011; Bloom et al. 2012a), the nature of the companion star that donates material is not yet clear. The various possibilities include the classical single degenerate (Whelan & Iben 1973) and double degenerate (Iben & Tutukov 1984; Webbink 1984) scenarios, as well as more contemporary variations on these themes. There is a varying degree of evidence supporting both sce-

⋆ E-mail:Yen-Chen.Pan@astro.ox.ac.uk

narios (e.g., Sternberg et al. 2011; Dilday et al. 2012; Schaefer & Pagnotta 2012); for a recent review see Maoz et al. (2013). A better understanding of SN Ia progenitors would likely strengthen their continuing use as cosmological probes (e.g., Riess et al. 1998; Perlmutter et al. 1999; Kessler et al. 2009; Riess et al. 2007; Sullivan et al. 2011; Rest et al. 2013; Betoule et al. 2014).

The host galaxies of SNe Ia are useful tools in these studies. For example, studying the global properties of the host environments of SNe Ia can reveal details of the progenitor systems and place broad constraints on their ages (e.g., Mannucci et al. 2005; Sullivan et al. 2006). Previous studies have also found significant correlations between SN Ia light curve parameters and luminosities, and the properties of their hosts (Hamuy et al. 1996, 2000; Gallagher et al. 2005, 2008; Kelly et al. 2010; Lampeitl et al. 2010; Sullivan et al. 2010; D'Andrea et al. 2011; Galbany et al. 2012; Johansson et al. 2013; Hayden et al. 2013; Childress et al. 2013a; Rigault et al. 2013; Pan et al. 2014). Intrinsically fainter SNe Ia (specifically those with faster light curves) are preferentially located in massive/older galaxies than in younger/lower-mass systems. Galaxies with stronger star-formation also tend to host slower, brighter SNe Ia than passive galaxies. From a cosmological perspective, 'corrected' SN Ia luminosities also show a dependence on various parameters correlated with host galaxy stellar mass ($M_{\rm stellar}$) and metallicity, in the sense that brighter SNe Ia tend to be found in massive/metal-rich galaxies. There are also emerging trends that massive, or metal-rich, galaxies host redder SNe Ia.

SN Ia spectral features are also important in understanding the properties of the progenitor system, providing the only direct tracer of the material in the SN ejecta. Work using the first large samples of maximum-light SN Ia spectra (e.g., Benetti et al. 2005; Branch et al. 2006) demonstrated the existence of several sub-classes of SN Ia events. Benetti et al. (2005) divided SNe Ia into three different groups according to their spectral properties: A 'FAINT' group including SN 1991bg-like events; a 'high-velocity group' (HVG), which present a high velocity gradient in their Si II λ6355 velocity evolution; and a 'low-velocity group' (LVG), which present a low velocity gradient in their Si II λ6355 velocities. Branch et al. (2006) grouped SNe Ia into four different groups according to the pseudo-equivalent-width (pEW) of Si II λ5972 and Si II λ6355 lines: A 'core-normal' group, which present homogeneous and intermediate pEWs; a 'shallow-silicon' group, which present low pEWs of both Si II λ6355 and Si II λ5972 lines and include SN 1991T-like events (taken together, the core-normal and shallow-silicon groups correspond to the Benetti et al. LVG); a 'broad-line' group (similar to the Benetti et al. HVG), which present normal pEWs of Si II λ5972 but higher pEWs of Si II λ6355; and a 'cool' group (similar to the Benetti et al. FAINT group).

Such studies indicate that SNe Ia are not drawn from a one-parameter family from the perspective of their spectral properties. Mazzali et al. (2007) studied the distribution of main elements in nearby SNe Ia and found the outer Si II λ6355 velocities are similar ($\lesssim$ 12000 km s^{-1}) for all SNe Ia except those defined as 'HVG' group, which show much higher and dispersed Si II λ6355 velocities. Wang et al. (2009) divided SNe Ia into two groups according to the photospheric velocities measured from Si II λ6355 absorptions. They found that SNe Ia with high Si II λ6355 velocities (high-$v_{\rm Si\,II}$; defined as $v_{\rm Si\,II} \gtrsim 12,000\,{\rm km\,s^{-1}}$) have a different extinction law than normal-velocity events (normal-$v_{\rm Si\,II}$; defined as $v_{\rm Si\,II} < 12,000\,{\rm km\,s^{-1}}$). By applying different values of R_V to each group, the dispersion in the corrected SN peak luminosities can be reduced. Many spectral indicators have also been found to correlate with SN luminosity, and can be used for distance estimation (Nugent et al. 1995; Hachinger et al. 2006; Bailey et al. 2009; Blondin et al. 2011; Silverman et al. 2012a).

However, there are fewer studies addressing the relationship between SN Ia spectral features and their host galaxies. Early work (Branch & van den Bergh 1993) showed that, when considering the full range of SNe Ia including subluminous events, SNe with the lowest Si velocities tended to explode in early-type galaxies. Foley (2012) studied the relation between Ca II H&K velocity and host $M_{\rm stellar}$, and found SNe Ia in massive galaxies have lower Ca II H&K velocities, although Maguire et al. (2012) suggested this could be caused by underlying relations between light-curve width and $M_{\rm stellar}$ (e.g., Sullivan et al. 2010), and between light-curve width and Ca II H&K velocity (see Maguire et al. 2012, 2014). Wang et al. (2013) found that high-$v_{\rm Si\,II}$ SNe Ia and normal-$v_{\rm Si\,II}$ SNe Ia may originate from different populations with respect to their radial distributions in their host galaxies. High-$v_{\rm Si\,II}$ SNe Ia tend to concentrate in the inner regions of their host galaxies, whereas the normal-$v_{\rm Si\,II}$ SNe Ia span a wider range of radial distance. Their result was interpreted as evidence for the existence of two distinct populations of SNe Ia.

As well as photospheric spectral features, 'high-velocity features' (HVFs) in SN Ia spectra, particularly in the Ca II near-infrared triplet, have also been studied (Wang et al. 2003; Gerardy et al. 2004; Mazzali et al. 2005a,b; Tanaka et al. 2006, 2008; Patat et al. 2009; Childress et al. 2013b; Marion et al. 2013; Childress et al. 2014). The physical origin of these HVFs is not yet clear, but it is generally thought to be related to an abundance or density enhancement in the SN ejecta, or interactions between the SN ejecta and a circumstellar medium (CSM) local to the SN. Some interesting properties have been found for these HVFs. For example, Childress et al. (2014) show the strength of the HVFs is connected to the decline rate of the SN light curve: slower declining SNe have stronger HVFs. They also found SNe Ia with stronger HVFs have lower Si II λ6355 photospheric velocities, while the high-$v_{\rm Si\,II}$ SNe Ia discussed above show no distinct HVFs in their maximum-light spectra. HVFs could also provide different angles to investigate the properties of CSM local to the SN. Sternberg et al. (2011) and Maguire et al. (2013) used the narrow Na I D features as probes for CSM and found the SNe presenting blue-shifted Na I D tend to be found in late-type galaxies. Foley et al. (2012) found these SNe with blue-shifted Na I D generally have higher ejecta velocities and redder colours at maximum light. Understanding the properties of these HVFs could provide some clues to their relations with any CSM and therefore the SN progenitor system.

In this paper, we use spectroscopic measurements of 122 low-redshift SNe Ia discovered by the Palomar Transient Factory (PTF) to investigate the relation between SN Ia spectroscopic properties and the SN host galaxies. In particular, we focus on the properties of the Si II λ6355 and Ca II near infrared absorptions. The spectral data and the measurements themselves are presented in a companion paper (Maguire et al. 2014), while the host parameters were determined using both photometric and spectroscopic data following Pan et al. (2014). In particular, we measure the SN–host galaxy offset, the host galaxy stellar mass ($M_{\rm stellar}$), the host star-formation rate (SFR), the host gas-phase/stellar metallicities, and the host mean stellar age.

A plan of the paper follows. In Section 2 we introduce the selection of our SN Ia spectral sample and the determination of host parameters, and Section 3 discusses the spectral measurements. In Section 4 we show the results found between SN Ia spectral properties and host parameters. The discussion and conclusion are presented in Section 5 and Section 6. Throughout this paper, we assume $\rm H_0 = 70\,km\,s^{-1}\,Mpc^{-1}$ and a flat universe with $\Omega_{\rm M} = 0.3$.

2 DATA

We begin by introducing the sample used in this work, including the sample selection, SN light curve fitting and the determination of host parameters.

2.1 The SN sample

The SNe Ia used in this work were discovered by the Palomar Transient Factory (PTF), a project designed to explore the optical transient sky using the CFH12k wide-field survey camera mounted on the Samuel Oschin 48-inch telescope (P48) at the Palomar Observatory (Rahmer et al. 2008; Rau et al. 2009; Law et al. 2009). PTF searched in both R and g-band filters (hereafter $R_{\rm P48}$ and $g_{\rm P48}$), and discovered $\sim$ 1250 spectroscopically confirmed SNe Ia during its operation from 2009–2012. SN candidates were identified in image subtraction data and ranked using a machine learning algorithm (Bloom et al. 2012b), and visually confirmed by either members of the PTF collaboration or via the citizen science project 'Galaxy Zoo: Supernova' (Smith et al. 2011).

SN detections were then spectroscopically confirmed and followed-up using a variety of facilities. These included: The William Herschel Telescope (WHT) and the Intermediate dispersion Spectrograph and Image System (ISIS), the Palomar Observatory Hale 200-in and the double spectrograph (DBSP; Oke & Gunn 1982), the Keck-I telescope and the Low Resolution Imaging Spectrometer (LRIS; Oke et al. 1995), the Keck-II telescope and the DEep Imaging Multi-Object Spectrograph (DEIMOS; Faber et al. 2003), the Gemini-N telescope and the Gemini Multi-Object Spectrograph (GMOS; Hook et al. 2004), the Very Large Telescope and X-Shooter (Vernet et al. 2011), the Lick Observatory 3m Shane telescope and the Kast Dual Channel Spectrograph (Miller & Stone 1993), the Kitt Peak National Observatory 4m telescope and the Ritchey-Chretien Spectrograph, and the University of Hawaii 88-in and the Supernova Integral Field Spectrograph (SNIFS; Lantz et al. 2004). All of the spectra used in this paper are available from the WISeREP archive (Yaron & Gal-Yam 2012), and are presented in detail in Maguire et al. (2014). Multi-colour light curves were not obtained by default for all SNe; instead they were assembled in g, r and i via triggered observations on other robotic facilities, e.g. the Liverpool Telescope (LT; Steele et al. 2004), the Palomar 60-in (P60) and the Las Cumbres Observatory Global Telescope Network (LCOGT; Brown et al. 2013) Faulkes telescopes (FTs).

Table 1. The SN sample selection in this work.

	Criterion	Num. of SNe left
PTF parent sample	–	1249
Redshift cut	$z < 0.09$	527
Spectral phase cut	$-5\,\rm d \leqslant t \leqslant 5\,d$	160
Redshift derived from host	–	143
LC quality cut	–	133
Spectrum quality cut	–	122
(In SDSS)	–	100

We are interested in studying SNe Ia with well-observed optical spectra near maximum light, and measuring their key spectral features. Thus we make several selection cuts on the parent PTF sample. In detail, these are as follows.

We first restrict our primary sample to those events with redshift of $z < 0.09$ (the final redshift distribution can be seen in Fig. 1). This same redshift cut was made in Pan et al. (2014), and avoids most Malmquist-bias selection effects (the median redshift of PTF SNe Ia is $\sim$ 0.1). It also ensures that the Ca II near infrared triplet that we study here is included in the spectral coverage (typically 3500 – 9000 Å). Secondly, we restricted the phases of SN spectroscopic observations to be within 5 rest-frame days relative to B-band maximum light, where the variation in the SN spectral velocities with phase show only a relatively mild and linear trend (discussed further in Section 3.2). We then restrict to the SNe where the redshifts can be estimated from host galaxy features rather than from SN template fitting, as spectral velocities are significantly more uncertain in the latter case. Finally, we exclude 21 SNe Ia from our sample which have only a poor quality (low S/N) spectrum or light curve. In total, 122 events passed the above criteria and enter our final sample. We summarise the sample selection in Table 1.

Of the 122 SNe Ia, 100 have host galaxies and available *ugriz* photometry in the Sloan Digital Sky Survey (SDSS) Data Release 10 (DR10; Ahn et al. 2013), which we use for an $M_{\rm stellar}$ determination (Section 2.2). A further two events lie outside of the SDSS footprint but their $M_{\rm stellar}$ can be determined using LT images taken as part of the SN photometric follow-up campaign. The details of calibrating these LT photometry can be found in Pan et al. (2014). The remainder of the 20 SNe without multi-colour photometric host data lie outside of the SDSS footprint.

The SiFTO light curve fitting code (Conley et al. 2008) was used to fit the SN light curves. The SN stretch (s), $B-V$ colour at B-band maximum light ($\mathcal{C}$), the rest-frame B-band apparent magnitude at maximum light (m_B), and the time of the maximum light in the rest-frame B-band are determined. Further details about the SN light curve fitting can be found in Pan et al. (2014).

2.2 Host galaxy properties

The main aim of this work is to investigate the relations between SN Ia spectral properties and their host parameters. The host stellar mass ($M_{\rm stellar}$) and SN offset were deter-

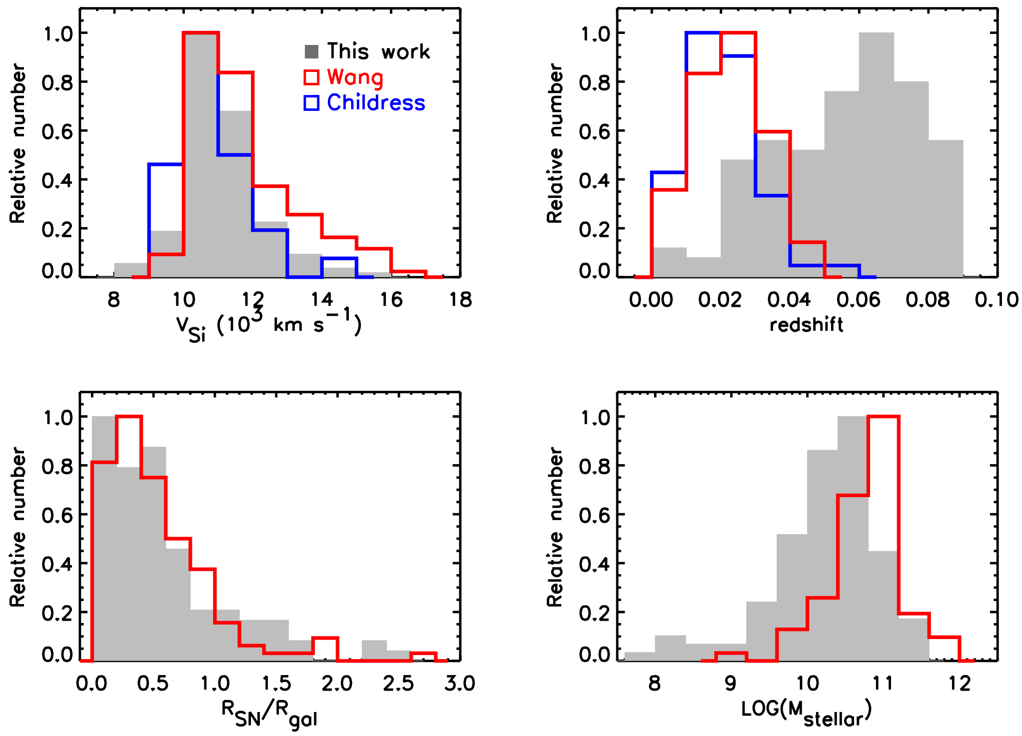

Figure 1. The distribution of the SN Si II $\lambda6355$ velocity, redshift, host galaxy offset, and host stellar mass ($M_{\rm stellar}$) of our sample (filled histogram). For comparison, the sample used in Wang et al. (2013) and Childress et al. (2014) are also shown in red and blue, respectively.

mined using the photometric data, and some of the hosts in our sample also have spectral parameters as measured in Pan et al. (2014). The detailed determination of host parameters were described in Pan et al. (2014). We summarise briefly as follows.

We determined the host $M_{\rm stellar}$ and star-formation rate (SFR) using the photometric redshift code Z-PEG (Le Borgne & Rocca-Volmerange 2002). Z-PEG fits the observed colour of the galaxies with galaxy Spectral Energy Distributions (SEDs) from 9 different spectral types (SB, Im, Sd, Sc, Sbc, Sb, Sa, S0 and E). Milky Way extinction is corrected for, and a further foreground dust screen varying from $E(B-V)=0$ to 0.2 mag in steps of 0.02 mag is fit. Throughout the paper a Salpeter (1955) Initial Mass Function (IMF) is assumed.

Of the 122 SN Ia host galaxies studied in this work, 41 events were studied in Pan et al. (2014), and therefore have well-measured spectral SFRs, gas-phase/stellar metallicities, and stellar ages. For these objects, the codes PPXF (Cappellari & Emsellem 2004) and GANDALF (Sarzi et al. 2006) were used to fit the host spectrum based on the stellar templates provided by the MILES empirical stellar library (Sánchez-Blázquez et al. 2006; Vazdekis et al. 2010). The potential AGN hosts in our sample were identified using the diagnostic studied by Baldwin, Phillips, & Terlevich (1981) (the so-called BPT diagram) with the criterion proposed by Kewley et al. (2001), and are not used for further emission-line analyses. The SFR is determined from the Hα luminosity based on the conversion of Kennicutt (1998). Following the procedure described in Kewley & Ellison (2008), we adopt the metallicity calibration studied by (Pettini & Pagel 2004, hereafter PP04) to calibrate the gas-phase metallicity. The 'N2' method (using the line ratio [N II] $\lambda6584$/Hα) in PP04 calibration is used. The mass-weighted stellar metallicity and age are determined using the 'full spectrum fitting' method, and PPXF is used to fit the stellar continuum of our host spectra. The stellar metallicity and age were then estimated by using a weighted average of the model templates.

We also measure the SN offset ($R_{\rm SN}$) from its host galaxy. $R_{\rm SN}$ is defined as the separation (i.e., projected radial distance) between the SN position and the host galaxy centre. The coordinates of the SN position were measured as a product of the P48 SN photometry procedures, and the host centre was determined using SEXTRACTOR (Bertin & Arnouts 1996) on the $R_{\rm P48}$ or $g_{\rm P48}$ reference images. We examine the potential hosts in the reference images by cross-checking the same field in the SDSS database; therefore we only measured the hosts which are covered by the SDSS footprint. For two SNe in our sample, we were not able to constrain the host positions as they were either too close to a bright star or in a very crowded field. This gave $R_{\rm SN}$ measures for 98 SNe.

These offsets are projected offsets, and so we investigate the possibility of deprojecting the offsets using our data. We can approximately deproject the SN offset using the position angle and axial ratio of the host galaxy measured by SEXTRACTOR (following the procedure described in Hakobyan et al. 2009). This correction is only valid for disk galaxies with moderate inclinations, and no corrections should be made for elliptical galaxies or disk galaxies with very large inclinations (i.e., nearly edge-on). Compared to the $z<0.05$ host galaxies studied in Wang et al. (2013), our host galaxies are generally more distant (Fig. 1) and smaller in their ap-

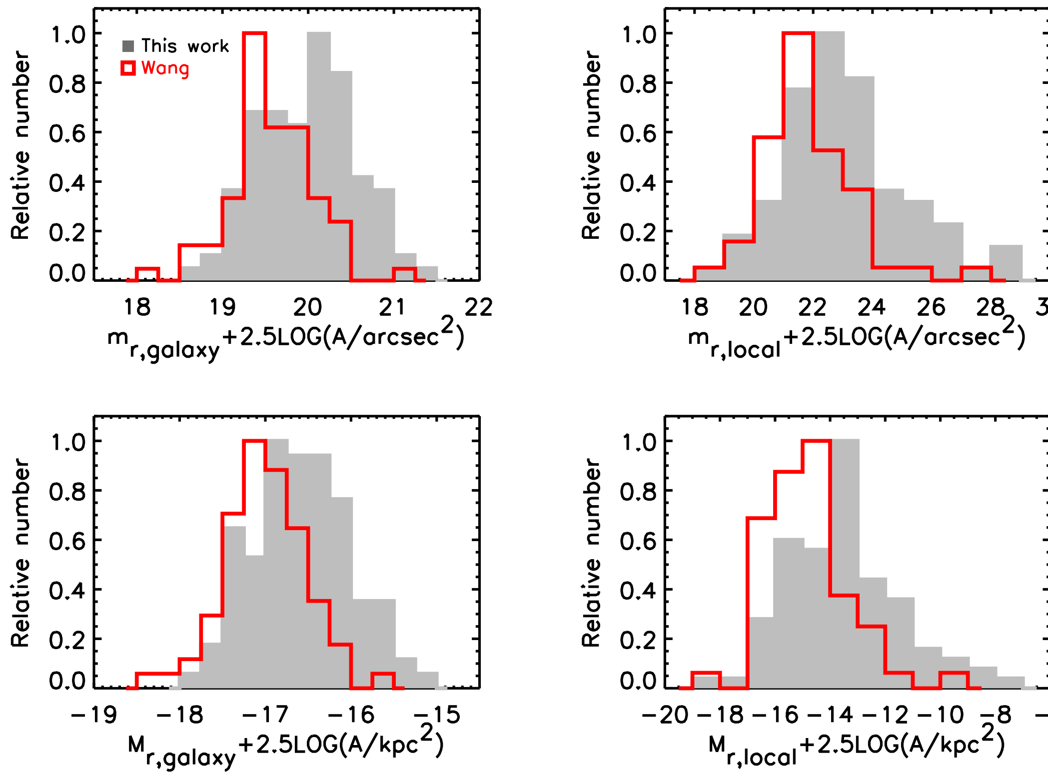

Figure 2. The comparison of host galaxy surface brightness from the SNe Ia in this work and that of Wang et al. (2013). Top panels: The distribution of surface brightness considering the whole galaxy (left panel) and the local region (a circle of radius 1″) at the SN position (right panel), respectively. The surface brightness is computed as $m_r + 2.5 \log A$, where A defines an area which encloses either the whole galaxy or the local region at the SN position. The enclosed area is in units of arcsec^2. Bottom panels: The same as the top panels, but considering the absolute magnitude (M_r) with enclosed area in units of kpc^2.

parent sizes. This introduces difficulties in classifying these galaxies and thus further increases the uncertainties in deprojecting the SN offsets. Furthermore, we found our results presented in later sections are not sensitive to the correction, and therefore no deprojection is applied for the host galaxies in this work.

We also measure a typical size of each of the host galaxies $\mathrm{R_{gal}}$, defined as the radius at which 90% of the flux from the galaxy is enclosed. We then use $\mathrm{R_{gal}}$ to normalise the SN offset. This is similar to the approach of Wang et al. (2013) but differs in detail; they use the $B = 25\,\mathrm{mag\,arcsec^{-2}}$ isophote as $\mathrm{R_{gal}}$. As this definition may introduce a redshift-dependent bias in the sizes measured, we do not attempt to replicate this measure on our R_{P48} and g_{P48} images.

Finally, we determined the surface brightness of our host galaxies and those from Wang et al. (2013) using SDSS r-band images. The galaxy surface brightness is computed as $m_r + 2.5 \log A$, where A represents the area of the ellipse which encloses the whole galaxy (in units of arcsec^2), and m_r is the apparent magnitude of the host galaxy determined by integrating the total counts enclosed within that ellipse (FLUX_AUTO in SEXTRACTOR). We also compute a 'local' surface brightness by integrating the total counts within a circular aperture of radius 1″ centred at the SN position. We then express the surface brightness in units of absolute magnitude (M_r) per kpc^2. The results can be found in Fig. 2.

3 SPECTRAL MEASUREMENTS

In this section, we discuss our method to measure the SN spectral features. The key features of interest are the pseudo-equivalent widths (pEW) and velocities of Si II λ6355 and the Ca II near infrared (NIR) triplet.

3.1 Line measurement

A complete description of the spectral feature measurement techniques can be found in Maguire et al. (2014). The method is similar to that of Childress et al. (2014), but with some differences, and developed independently. Here we briefly summarise our procedure.

We started by fitting the Si II λ6355 doublet, a prominent line in SN Ia spectra with little contamination from other features. We correct the SN spectrum into the rest frame, define (by hand) continuum regions on either side of the feature, and fit a straight line pseudo-continuum across the absorption feature. The feature is then normalised by dividing it by the pseudo-continuum. A double-Gaussian fit is performed to the normalised Si II λ6355 doublet line in velocity space using the MPFIT package (Markwardt 2009). The centres of the two Gaussians have a fixed velocity difference corresponding to the difference in the wavelengths of the doublet (λ6347Å and λ6371Å) and the same width. The relative strengths of the individual line components are fixed to be equal by assuming an optically thick regime (e.g., Chil-

Table 2. The gradient of the SN spectral feature evolution in this work.

Feature	Gradient
Si II λ6355 velocity	-32 ± 22 km s^{-1}d^{-1}
Ca II NIR velocity (PVF)	$+38 \pm 59$ km s^{-1}d^{-1}
Ca II NIR velocity (HVF)	-336 ± 80 km s^{-1}d^{-1}
Ca II NIR pEW (PVF)	$+3.2 \pm 1.1$ Å d^{-1}
Ca II NIR pEW (HVF)	-3.5 ± 2.1 Å d^{-1}

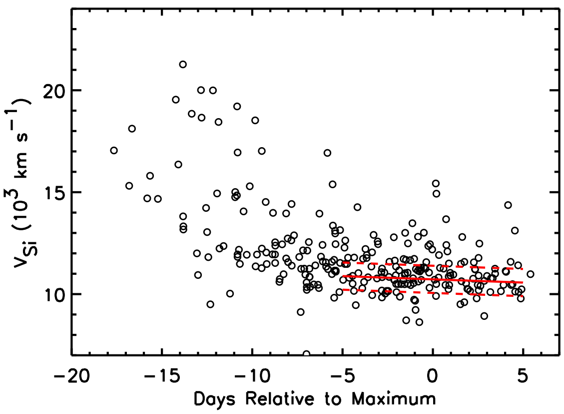

Figure 3. The Si II λ6355 velocity as a function of the phase of the SN Ia spectroscopic observation. The red solid line shows a linear fit to data with phases from −5 d to +5 d. The dashed lines show the 1-σ range relative to the fit.

dress et al. 2014; Maguire et al. 2014). The resulting fit then gives the velocity of the feature, together with the pEW.

We then fit the complex Ca II NIR feature. This is a more complicated task as the Ca II high-velocity component can be strong around SN maximum light, and thus we fit for both photospheric velocity and high-velocity components in the absorption complex. To achieve this, the Si II λ6355 velocity and width derived from previous fit are used as initial guesses for the photospheric component of the Ca II NIR line. We then require the velocity of the Ca II NIR photospheric component to be within 25% of the Si II λ6355 velocity, and the Ca II NIR high-velocity component to be larger than the Si II λ6355 velocity by at least 2000 km s^{-1}. No other constraints are applied during the fit.

To ensure our measurements of these absorption lines are not sensitive to the locations we selected for deriving the pseudo-continuum, we randomly move the red and blue pseudo-continuum regions by up to 10Å with respect to the original location, and re-fit the line profile. This random process is repeated 200 times. The final values reported in this work are the mean of the measurements from all the iterations, and the uncertainty is the standard deviation.

3.2 Phase evolution of spectral features

As discussed in Section 2.1, we restrict the phases of our PTF SN Ia spectral sample to be within 5 days of the B-band maximum light of the SN. Over this phase range, SN Ia spectral velocities generally show a mild and linear trend (e.g., Silverman et al. 2012b). This can also be seen in our sample in Fig. 3 (see also Maguire et al. 2014), which shows the Si II λ6355 velocity as a function of phase. We list the gradient of each spectral feature in this work in Table 2. However, the rate of phase evolution for these spectral features could show considerable diversity for different SNe Ia (Benetti et al. 2005; Blondin et al. 2012). Therefore we did not correct the SN spectral features using the gradients listed in Table 2, and instead chose to use the spectral measurements with the phases closest to the time of B-band maximum light. We found our results in later sections are not sensitive to the phase corrections.

3.3 Comparison with other samples

Fig. 1 and Fig. 2 show the comparison of the Si II λ6355 velocity ($v_{\mathrm{Si\,II}}$), redshift, normalised SN offset (R_{SN}/R_{gal}), M_{stellar} and surface brightness distributions between this work and the sample used in Wang et al. (2013) and Childress et al. (2014). Here, we only show the 123 'Branch-Normal' SNe Ia used in Wang et al. (2013). We determined the M_{stellar} for the hosts studied in Wang et al. (2013) using the same method described in Section 2.2, with 74 out of 123 events having available SDSS photometry for comparison to our sample.

The Wang et al. (2013) M_{stellar} distribution is very different from this work. This is almost certainly due to the selection of the SN sample used by Wang et al. (2013), which were discovered by the Lick Observatory Supernova Search (LOSS), designed as a galaxy-targeted survey. A Kolmogorov-Smirnov (K-S) test gives a < 1 per cent probability that the M_{stellar} distributions of Wang et al. (2013) and this work are drawn from the same underlying population.

We also see a large difference in the $v_{\mathrm{Si\,II}}$ distributions, with Wang et al. (2013) having a larger fraction of SNe Ia with high $v_{\mathrm{Si\,II}}$. Our $v_{\mathrm{Si\,II}}$ distribution is consistent with that of Childress et al. (2014). We find no evidence for a redshift evolution in $v_{\mathrm{Si\,II}}$ in our sample, making the small redshift difference between our sample and that of Wang et al. (2013) unlikely to drive the offset in Fig. 1. We discuss the possible origin of the $v_{\mathrm{Si\,II}}$ discrepancy in Section 4.1.2. The SN radial distribution of this work is consistent with that of Wang et al. (2013), despite the slightly different definitions (Section 2.2).

Our sample also differs from Wang et al. (2013) in the surface brightness distributions of the host galaxies (Fig. 2). The majority of the host galaxies sampled by Wang et al. (2013) have high surface brightnesses, where in this work we sample galaxies with both high and low surface brightness. A K-S test gives a $< 0.01\%$ probability that the host galaxies studied from Wang et al. (2013) and this work are drawn from the same population with respect to their surface brightness. Similar results were also found when investigating the local surface brightness at the SN position, with the sample in Wang et al. (2013) again biased toward those with high surface brightness. However, we find no evidence that PTF is biased against events on a high-surface brightness background; the bright ends of the surface brightness distributions are similar between PTF and Wang et al. (2013).

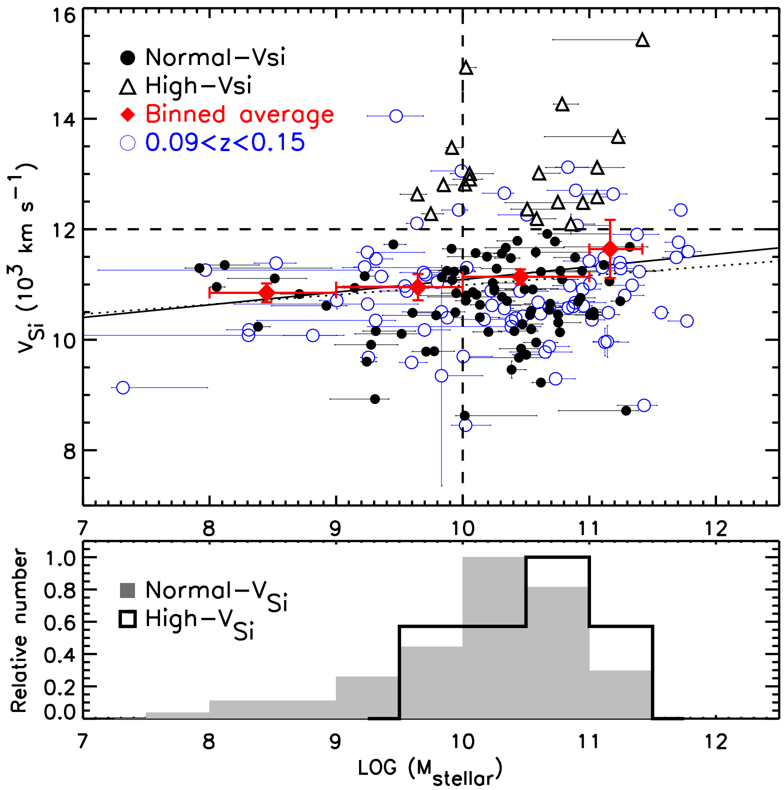

Figure 4. The Si II $\lambda6355$ velocities ($v_{\rm Si\,II}$) as a function of $M_{\rm stellar}$. The high-$v_{\rm Si\,II}$ SNe Ia (with $v_{\rm Si\,II} \geqslant 12000\,{\rm km\,s^{-1}}$) are shown as open triangles, and the normal-$v_{\rm Si\,II}$ SNe Ia are shown as filled circles. The red diamonds represent the mean velocities in bins of $M_{\rm stellar}$, and their error bars are the width of the bins and the error on the mean. The vertical and horizontal dashed lines represent the criterion used to split the sample in velocity and $M_{\rm stellar}$ space, respectively. The solid line is the linear fit to the data in the plot (filled circles plus open triangles). We overplot the SNe with $0.09 < z < 0.15$ in open blue circles for comparison. The linear fit to all the data (including those $0.09 < z < 0.15$) is shown in dotted line. The bottom histograms show the $M_{\rm stellar}$ distributions of high-$v_{\rm Si\,II}$ and normal-$v_{\rm Si\,II}$ SNe Ia.

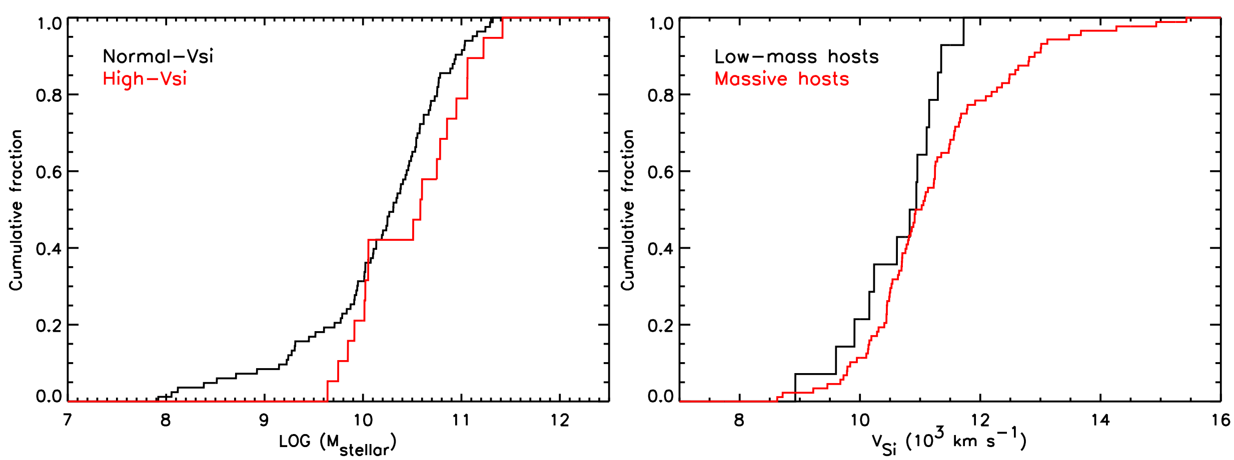

Figure 5. Left panel: The cumulative fractions of host $M_{\rm stellar}$ of high-$v_{\rm Si\,II}$ and normal-$v_{\rm Si\,II}$ SNe Ia. Right panel: The cumulative fractions of $v_{\rm Si\,II}$ of SNe Ia in high- and low-mass host galaxies.

4 RESULTS

We now turn to the main results of our study. We split our analysis into two parts. The first concerns the properties of the photospheric features and velocities, namely the Si II $\lambda6355$ and Ca II NIR photospheric velocities ($v_{\rm Si\,II}$ and $v_{\rm Ca\,II\,NIR}$). In this discussion we include trends for SNe with very high $v_{\rm Si\,II}$, which we denote high velocity events and, following Wang et al. (2013), define as $v_{\rm Si\,II} \geqslant 12000\,{\rm km\,s^{-1}}$. The second part concerns the strength of the high-velocity features present in the Ca II NIR absorption.

4.1 Photospheric features and host galaxy parameters

4.1.1 Stellar mass

We begin by examining trends with host galaxy stellar mass ($M_{\rm stellar}$). Fig. 4 shows $v_{\rm Si\,II}$ as a function of $M_{\rm stellar}$. There is a broad trend that high-$v_{\rm Si\,II}$ SNe Ia tend to reside in massive galaxies, whereas the normal-$v_{\rm Si\,II}$ SNe Ia ($v_{\rm Si\,II} < 12000\,{\rm km\,s^{-1}}$) are found in galaxies of all mass. In our sample, high-$v_{\rm Si\,II}$ SNe Ia only occur in galaxies with $\log(M_{\rm stellar}) > 9.5$. Fig. 5 (left panel) shows the cumulative distribution function of host galaxy $M_{\rm stellar}$ for both high- and normal-$v_{\rm Si\,II}$ SNe Ia. The two distributions are different particularly at the low-$M_{\rm stellar}$ end. The cumulative distribution function of $v_{\rm Si\,II}$ for SNe Ia in high-$M_{\rm stellar}$ ($\log(M/M_{\odot}) > 10$) and low-$M_{\rm stellar}$ ($\log(M/M_{\odot}) < 10$) hosts is also shown in Fig. 5 (right panel). The distribution of high-$M_{\rm stellar}$ hosts is different from low-$M_{\rm stellar}$ hosts due to additional SNe at high $v_{\rm Si\,II}$.

The classical K-S test is less sensitive when testing two distributions that vary mainly in their tails, and indeed gives a p-value of 0.25 that the normal- and high-$v_{\rm Si\,II}$ SN $M_{\rm stellar}$ distributions are drawn from the same underlying population (i.e., they are not two distinct populations). The same test gives a p-value of 0.21 that low-$M_{\rm stellar}$ and high-$M_{\rm stellar}$ hosts have $v_{\rm Si\,II}$ distributions drawn from the same population. Drawing 19 SNe Ia, the size of the high-$v_{\rm Si\,II}$ sample, with replacement and at random from the full PTF sample, only in 3.1% of iterations do all the selected SNe have $M_{\rm stellar}$ greater than $4.36 \times 10^9\,M_{\odot}$ (the minimum $M_{\rm stellar}$ of the high-$v_{\rm Si\,II}$ SNe Ia in this work). Finally, a linear fitting performed by LINMIX (Kelly 2007) shows a non-negative slope at 87% probability.

These results are suggestive, but not conclusive, that high-$v_{\rm Si\,II}$ SNe Ia prefer high-$M_{\rm stellar}$ host galaxies, and of a more general relationship between $v_{\rm Si\,II}$ and $M_{\rm stellar}$. We investigate if the trend holds when adding additional high-redshift $0.09 \leqslant z < 0.15$ PTF SNe Ia (our primary sample has $z < 0.09$; Section 2.1). This larger sample has more significant trends: the linear fitting prefers a non-negative slope at 93% probability.

Previous studies found some evidence that $v_{\rm Ca\,II\,H\&K}$ correlates with $M_{\rm stellar}$, in the sense that SNe Ia in more massive galaxies tend to have lower $v_{\rm Ca\,II\,H\&K}$ (e.g., Foley 2012; Maguire et al. 2012); note this is opposite to the trends with $v_{\rm Si\,II}$ in Fig. 4). Maguire et al. (2012) suggested that this trend is caused by an underlying relationship between SN light curve shape and Ca II H&K velocity, in the sense that SNe Ia with higher stretches tend to have higher Ca II H&K velocities. They found the trend between Ca II H&K velocity and $M_{\rm stellar}$ disappeared after removing the correlation between SN light curve shape and Ca II H&K velocity.

However, Foley (2013) argued the contribution of Si II λ3858 line in Ca II H&K feature is important, and may make the measurement of the Ca II H&K line uncertain. They suggested the blue component of the Ca II H&K feature is caused by the Si II λ3858 feature for most SNe Ia, and that therefore the correlation between SN light curve shape and $v_{\rm Ca\,II\,H\&K}$ observed in Maguire et al. (2012) could be due to the strong correlation between Si II λ3858 and excitation temperature, and therefore the SN light curve shape. Childress et al. (2014) found the HVFs are stronger in higher stretch SNe Ia, supporting the idea proposed by Maguire et al. (2012). However, they also showed the Si II λ3858 line does have some impact on the Ca II H&K line. Taken together, these results imply the trend between $v_{\rm Ca\,II\,H\&K}$ and $M_{\rm stellar}$ may not be unambiguously caused by an intrinsic property of Ca II feature itself.

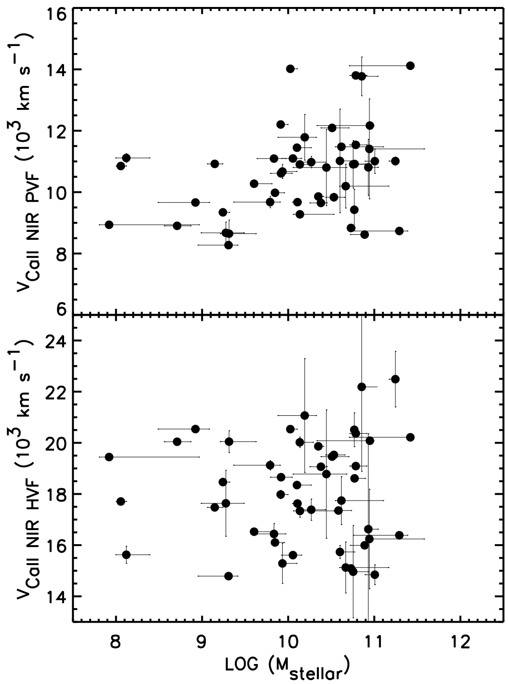

Figure 6. The upper panel shows the Ca II NIR velocities of photospheric feature (PVF) component as a function of $M_{\rm stellar}$. The lower panel shows the Ca II NIR velocities of high-velocity feature (HVF) component as a function of $M_{\rm stellar}$.

Clearly a problem with these analyses is the use of the Ca II H&K feature, which is a difficult feature to model accurately. Here we use Ca II NIR line instead, as it provides a cleaner measurement of Ca II velocity without contamination from other features (e.g., Si); we are also able to more easily decompose the high-velocity and photospheric-velocity components. Fig. 6 shows the Ca II NIR velocity of these photospheric and high-velocity components as a function of $M_{\rm stellar}$. Similar to our $v_{\rm Si\,II}$ analysis, SNe with the highest photospheric $v_{\rm Ca\,II\,NIR}$ also tend to reside in massive galaxies. The high-velocity $v_{\rm Ca\,II\,NIR}$ shows no significant trend with $M_{\rm stellar}$, although there is a suggestion that SNe with low $v_{\rm Ca\,II\,NIR}$ are deficient in lower-mass galaxies. In our companion paper, Maguire et al. (2014), we show that SNe Ia with strong HVFs in the Ca II NIR feature relative to photospheric Ca II generally have higher Ca II velocities. If the hosts with lower $M_{\rm stellar}$ ($\log {\rm M} < 10$) are dominated by SNe with strong HVFs (as we will see in Section 4.2), we will expect the SNe in low $M_{\rm stellar}$ galaxies to have higher Ca II NIR HVF velocities. This may also explain the tendency for the low-mass galaxies in our sample to lack SNe with low Ca II NIR HVF velocities.

4.1.2 SN offset

Wang et al. (2013) found evidence for two distinct popu-

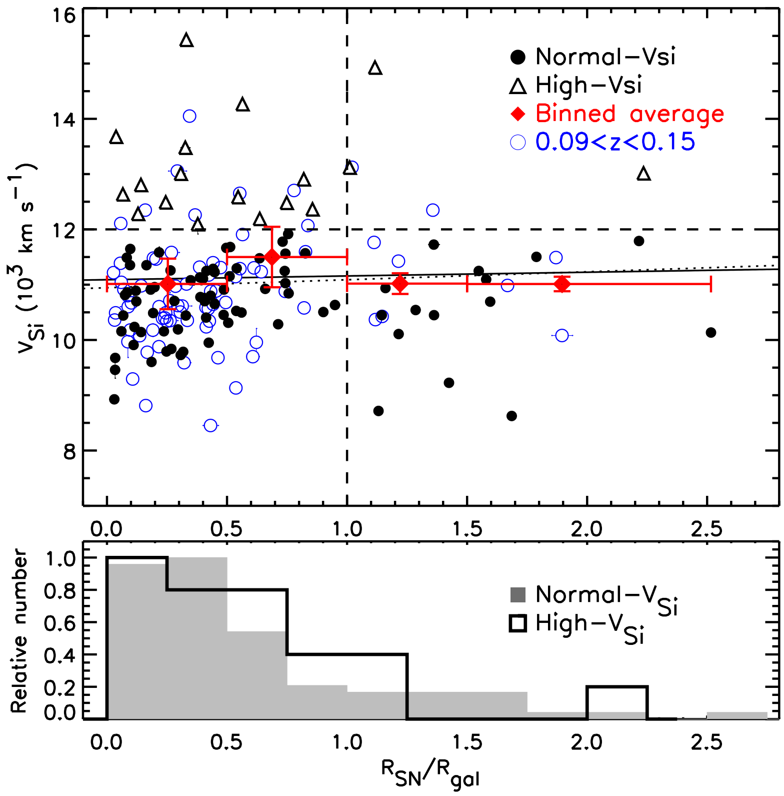

Figure 7. As Fig. 4, but considering the R_{SN}/R_{gal} ratio instead of $M_{stellar}$. R_{SN} and R_{gal} are defined in Section 2.2.

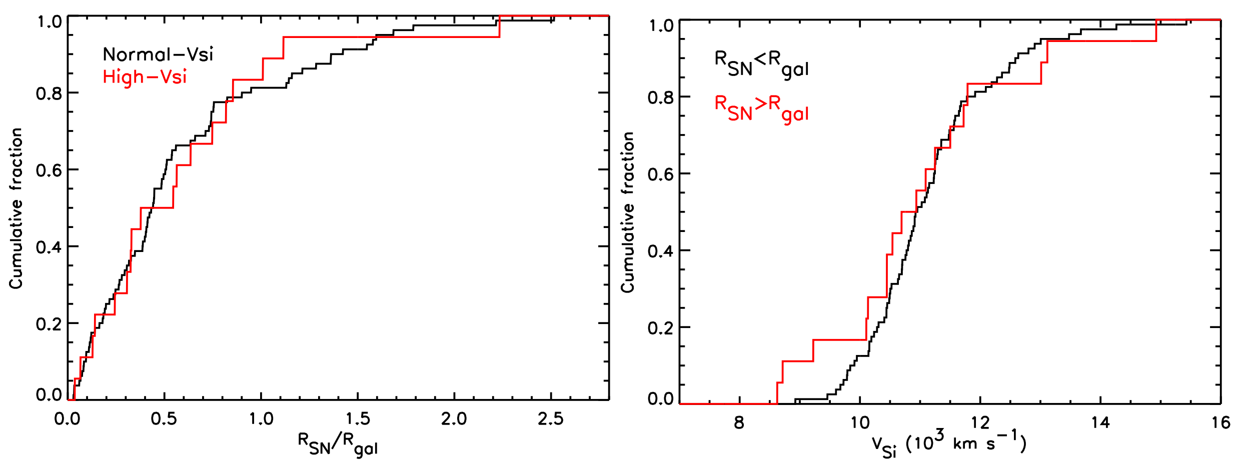

Figure 8. Left panel: The cumulative fractions of R_{SN}/R_{gal} of high-$v_{\rm Si\,II}$ and normal-$v_{\rm Si\,II}$ SNe Ia. Right panel: The cumulative fractions of in $v_{\rm Si\,II}$ of SNe Ia in larger radial distance and smaller radial distance.

lations of SNe Ia with respect to their radial distributions in the host galaxies. They found that the high-$v_{\rm Si\,II}$ SNe Ia are concentrated in the inner regions of their host galaxies, whereas the normal-$v_{\rm Si\,II}$ SNe Ia span a wide range of radial distance. We next examine this trend in our sample in Fig. 7, showing $v_{\rm Si\,II}$ as a function of the normalised SN offset, R_{SN}/R_{gal} (see Section 2.2). The high-$v_{\rm Si\,II}$ SNe Ia in the PTF sample also appear deficient in the outer regions of their hosts compared to the normal-$v_{\rm Si\,II}$ SNe Ia, which are found at all radii. The only high-$v_{\rm Si\,II}$ SN at a large radius (PTF09djc; $v_{\rm Si\,II}$= 13013 km s^{-1}, R_{SN}/R_{gal}= 2.2) resides in the outskirts of an extended galaxy, with no potential host found at the SN position to the SDSS photometric limit ($r \simeq 22$ mag).

However, in our sample the trend is not statistically significant. We found that the locations of 83% of the high-$v_{\rm Si\,II}$ SNe Ia and 81% of the normal-$v_{\rm Si\,II}$ SNe Ia are within $R_{SN}/R_{gal} = 1$, which implies the high-$v_{\rm Si\,II}$ SNe Ia are similar to the normal-$v_{\rm Si\,II}$ SNe Ia with respect to their radial distribution, although the normal-$v_{\rm Si\,II}$ SN sample size is much larger. Fig. 8 shows the cumulative distribution functions of R_{SN}/R_{gal} for high-$v_{\rm Si\,II}$ and normal-$v_{\rm Si\,II}$ SNe Ia, and $v_{\rm Si\,II}$ for SNe at $R_{SN}/R_{gal} > 1$ and $R_{SN}/R_{gal} < 1$. We do not see significant differences in the distributions; a K-S test

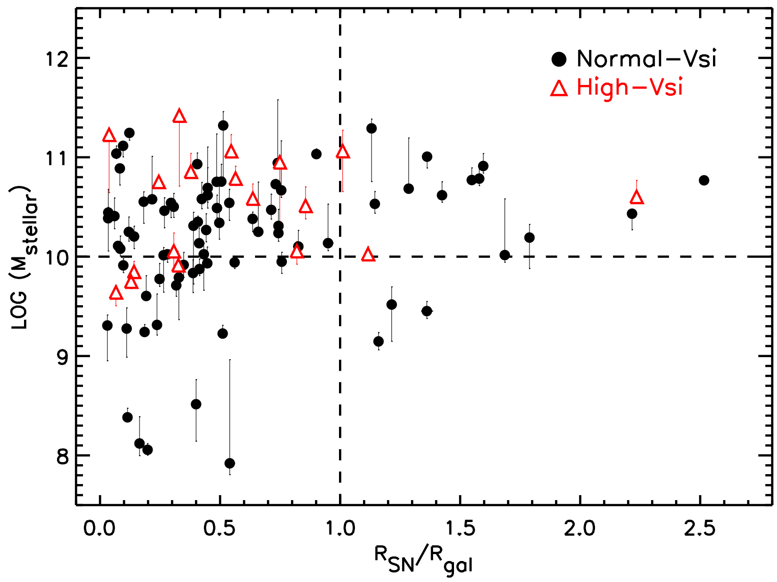

Figure 9. The host galaxy $M_{\rm stellar}$ as a function of $\rm R_{SN}/R_{gal}$. The data are colour-coded in terms of the Si II λ6355 velocity ($v_{\rm Si\,II}$): high-$v_{\rm Si\,II}$ SNe Ia (red) and normal-$v_{\rm Si\,II}$ SNe Ia (black).

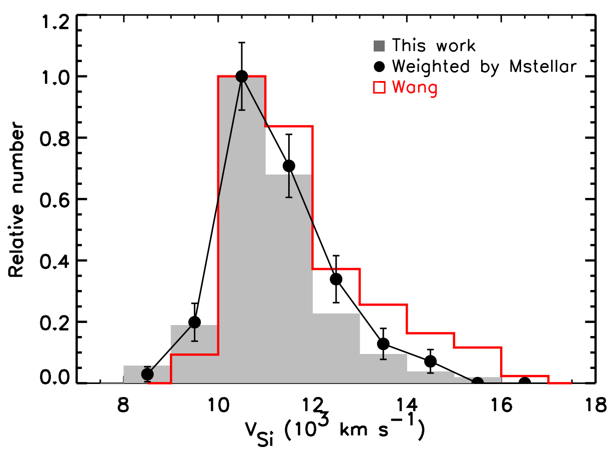

Figure 10. The comparison of the $v_{\rm Si\,II}$ distributions in the PTF sample (filled histogram) compared with the Wang et al. (2013) sample (open red histogram). The filled circles connected by solid lines show the distribution of our sample weighted by the $M_{\rm stellar}$ of Wang et al. (2013), in an attempt to account for the selection differences seen in Fig. 1.

gives p=0.87 that high-$v_{\rm Si\,II}$ SNe Ia and normal-$v_{\rm Si\,II}$ SNe Ia are drawn from the same population in $\rm R_{SN}/R_{gal}$. This value is larger than that for the Wang et al. (2013) sample (p = 0.005). Repeating the same analysis as Section 4.1.1 and randomly selecting 18 SNe from the full sample, in only 3.3% of cases do all the selected SNe have $\rm R_{SN}/R_{gal}$ smaller than 1.1 (the maximum $\rm R_{SN}/R_{gal}$ of the high-$v_{\rm Si\,II}$ SNe Ia). However, this test excludes the outlier PTF09djc. We see very similar results when including all PTF SNe Ia up to $z < 0.15$, and similar results when only considering SNe Ia in massive host galaxies. We thus conclude that there is no strong evidence in our sample that high-$v_{\rm Si\,II}$ SNe Ia prefer the inner regions of their host galaxies.

Fig. 9 shows the host $M_{\rm stellar}$ as a function of $\rm R_{SN}/R_{gal}$. The data points are colour-coded in terms of the Si II λ6355 velocities. This diagram provides us different angle to investigate the properties of the high-$v_{\rm Si\,II}$ SNe Ia. The high-$v_{\rm Si\,II}$ SNe Ia tend to occupy a parameter space which has both higher $M_{\rm stellar}$ and smaller $\rm R_{SN}/R_{gal}$, consistent with our earlier results.

One explanation for the differing level of significance, despite the similar overall sizes of this and the Wang et al. (2013) sample, is that the PTF sample has a smaller fraction of high-$v_{\rm Si\,II}$ SNe Ia (20%; 20 high-$v_{\rm Si\,II}$ SNe and 102 normal-$v_{\rm Si\,II}$ SNe) compared to Wang et al. (2013) (33%; 40 high-$v_{\rm Si\,II}$ SNe Ia and 83 normal-$v_{\rm Si\,II}$ SNe Ia). This may be because the Wang et al. (2013) sample is biased towards both massive galaxies and higher surface brightness galaxies (Fig. 1 and Fig. 2; Section 3.3), whereas PTF is untargeted. If high-$v_{\rm Si\,II}$ SNe Ia occur more frequently in massive galaxies (e.g., Fig. 4; Section 4.1.1), we would expect more high-$v_{\rm Si\,II}$ SNe Ia to be discovered in a galaxy-targeted survey such as LOSS.

We test this hypothesis by attempting to reproduce the $v_{\rm Si\,II}$ distribution of Wang et al. (2013) using the PTF sample, by matching the Wang et al. selection in $M_{\rm stellar}$. We generate synthetic SN samples by selecting 123 events (the size of the Wang et al. sample) from the PTF sample, with the probability of a SN being selected weighted by its $M_{\rm stellar}$, using the $M_{\rm stellar}$ distribution from Wang et al. (2013). We repeated this procedure 10,000 times and determined the mean $v_{\rm Si\,II}$ distribution. The result is shown in Fig. 10.

Weighting by $M_{\rm stellar}$ clearly alters the $v_{\rm Si\,II}$ distribution of our synthetic sample, as expected. The distribution in $v_{\rm Si\,II}$ between 8000 and 13000 km s^{-1}, after weighting by $M_{\rm stellar}$, is now consistent with Wang et al. (2013). However, the distribution is still inconsistent at $v_{\rm Si\,II} > 13000$ km s^{-1}. Thus although the selection bias in $M_{\rm stellar}$ may explain some of the difference, it is clear that either some other variable is also at work, or our tests of the selection effects do not capture all the effect.

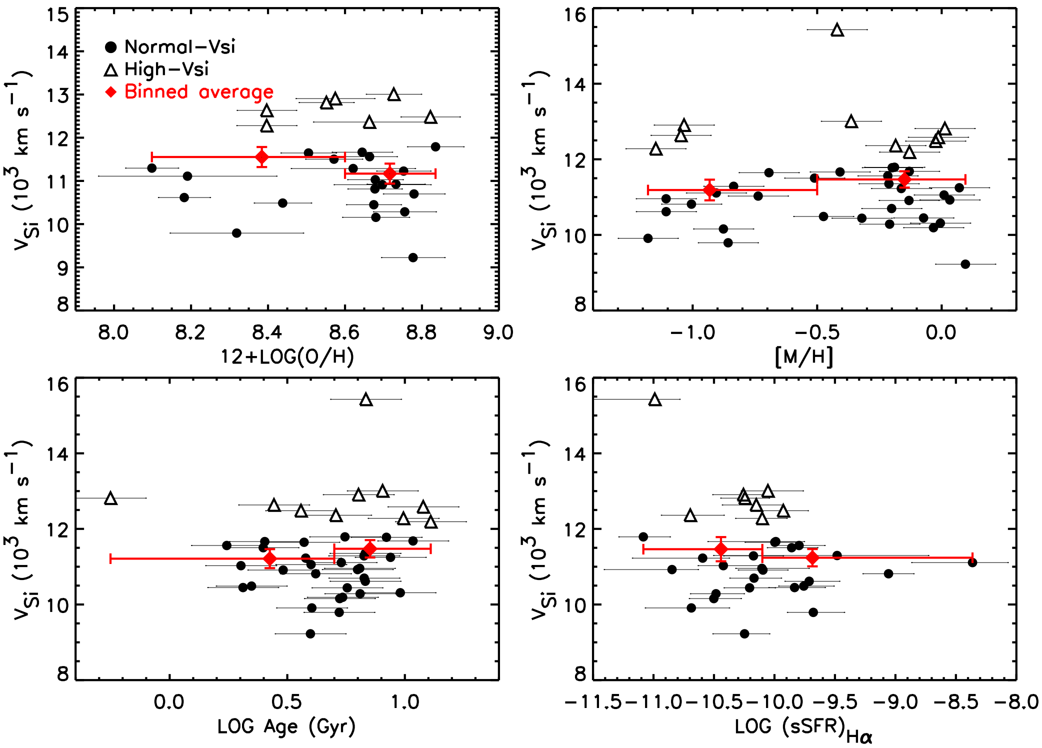

Figure 11. The Si II λ6355 velocity ($v_{\rm Si\,II}$) as a function of gas-phase metallicity (upper left), stellar metallicity (upper right), stellar age (lower left) and specific star-formation rate (lower right). The red diamonds represent the mean of $v_{\rm Si\,II}$ in bins of each of the host parameters, and the error bars are the width of the bins and the error of the mean.

4.1.3 Other host parameters

As discussed in Section 2.2, some of the host galaxies in our sample also have host spectral parameters measured in Pan et al. (2014). These include specific star formation rate (sSFR), gas-phase metallicity, stellar metallicity and stellar age, and in Fig. 11, we present the $v_{\rm Si\,II}$ as a function of these parameters. The sample size is smaller than for the investigations related to $M_{\rm stellar}$ or $R_{\rm SN}/R_{\rm gal}$, and we do not find any significant trends between $v_{\rm Si\,II}$ and these host properties.

4.2 High-velocity features and host parameters

We now discuss the HVFs seen in the Ca II NIR feature. Following the procedure in Childress et al. (2014), we quantify the strength of the HVFs using the ratio ($R_{\rm HVF}$) of the pEWs of the Ca II NIR high-velocity component to the pEW of the photospheric component. SNe Ia with a larger $R_{\rm HVF}$ will present stronger relative absorption in the high-velocity component compared to the photospheric component. We define SNe Ia with $R_{\rm HVF} > 1.0$ as having strong HVFs.

Fig. 12 shows $R_{\rm HVF}$ as a function of the SN stretch (s), $v_{\rm Si\,II}$, and $M_{\rm stellar}$ (see Maguire et al. 2014, for the correlation between $R_{\rm HVF}$ and stretch for the full PTF sample). We see a clear trend that nearly all SNe Ia with a large $R_{\rm HVF}$ have high stretches ($s \gtrsim 1.0$), as expected based on earlier work (Childress et al. 2014). This trend could be driven either by stronger HVFs in high-stretch SNe Ia, or by weaker photospheric features. Maguire et al. (2014) demonstrated that both effects are present: high-stretch SNe have both weaker photospheric features, and stronger HVFs. The former can be understood if high stretch SNe Ia have higher temperatures, and therefor a higher ionisation: photospheric Ca II is ionised to Ca III and thus the Ca II pEW becomes weaker.

There is one outlier in Fig. 12 with very high stretch but weak HVF: PTF09dhx ($s = 1.7$, $R_{\rm HVF} = 0.54$). By contrast, SNe Ia with high-$v_{\rm Si\,II}$ have relatively weak HVFs and intermediate stretches ($0.8 < s < 1.1$). We also confirm that SNe Ia with a large $R_{\rm HVF}$ have normal Si II λ6355 velocities ($v_{\rm Si\,II}$ $< 12000\,{\rm km\,s^{-1}}$), already noted by Childress et al. (2014). There is only one SN in our sample has both strong HVFs and high Si II λ6355 velocity (PTF10lot; $v_{\rm Si\,II}$= 12802 km s^{-1} and $R_{\rm HVF}$= 1.33). The lower panels of Fig. 12 show the relations between SN stretch, $M_{\rm stellar}$ and $R_{\rm HVF}$. In contrast to the high-$v_{\rm Si\,II}$ SNe Ia, which are likely to reside in massive galaxies, here we find that SNe Ia with a large $R_{\rm HVF}$ are preferentially found in low-mass galaxies. Thus SNe Ia with high-$v_{\rm Si\,II}$ appear different in terms of their host galaxies to SNe Ia with high-velocity Ca II NIR features.

In Fig. 13 we examine $R_{\rm HVF}$ as a function of the specific star-formation rate (sSFR) and $R_{\rm SN}/R_{\rm gal}$. Here we use the sSFR determined by Z-PEG, instead of using the Hα luminosity, to increase the sample size. The events with a large $R_{\rm HVF}$ all reside in strongly star-forming galaxies, and indeed nearly all SNe Ia in such galaxies display strong HVFs. By contrast, SNe Ia with high-$v_{\rm Si\,II}$ tend to reside in galaxies with intermediate sSFRs: log(sSFR) ~ -9.7. For the relation between $R_{\rm HVF}$ and $R_{\rm SN}/R_{\rm gal}$, we found all SNe Ia with a large $R_{\rm HVF}$ are located within $R_{\rm SN}/R_{\rm gal} = 1$ of their host galaxies. As we will see in Section 5.2, these HVFs mostly come from late-type galaxies (spirals or irregulars).

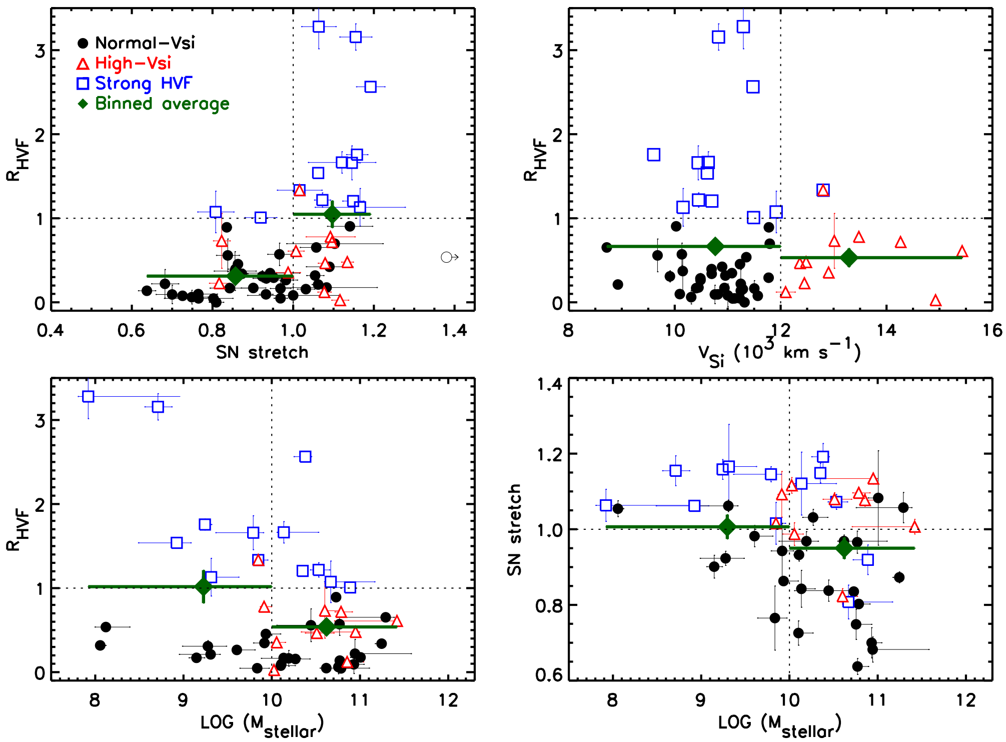

Figure 12. The ratio of the pEW of the high-velocity Ca II NIR feature to the photospheric Ca II feature, R_{HVF} as a function of various parameters. Upper left is the SN stretch, upper right the Si II λ6355 velocity, and lower left the $M_{stellar}$. The SN stretch is plotted against $M_{stellar}$ in the lower-right panel. Only SNe with Ca II NIR features are plotted. The solid circles, open triangles and open squares represent the normal-$v_{Si\,II}$ SNe Ia, high-$v_{Si\,II}$ SNe Ia and SNe Ia with a large R_{HVF}) respectively. The solid green diamonds represent the mean R_{HVF} in each bin. The open circle shows one outlier in the plot: PTF09dhx ($s = 1.7$, $R_{HVF} = 0.54$)

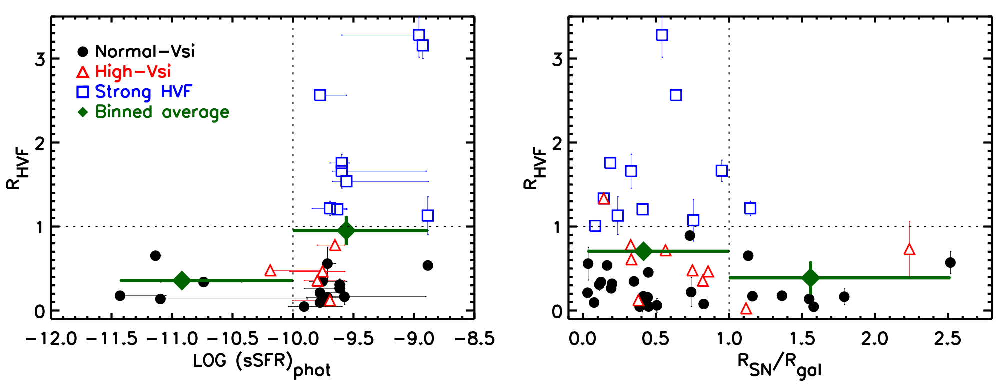

Figure 13. The same as Fig. 12 but with the sSFR derived from Z-PEG (left) and R_{SN}/R_{gal} (right).

This strongly implies that SNe Ia with HVFs are less likely to originate from old populations residing in galactic haloes distant from the host centre.

5 DISCUSSION

5.1 Silicon velocity and metallicity

Wang et al. (2013) found that high-$v_{Si\,II}$ SNe Ia appear concentrated in the inner regions of their host galaxies, whereas normal-$v_{Si\,II}$ SNe Ia span a wider range of radial distance. Observations have shown that negative metallicity gradients are common in both the Milky Way and many external galaxies, in the sense that the heavy-element abundances decrease systematically outward from the centre of galaxies (Henry & Worthey 1999). Therefore we would expect these high-$v_{Si\,II}$ SNe Ia are more likely to originate from metal-rich (and older) populations. In this work we did not find any significant trends between high-$v_{Si\,II}$ SNe Ia and radial position. However, we did observe a stronger trend that high-$v_{Si\,II}$ SNe Ia tend to explode in more massive galaxies. According to the galaxy mass-metallicity relation (Tremonti et al. 2004; Kewley & Ellison 2008), massive galaxies are generally more metal-rich than low-mass galaxies, and thus the stellar populations in the inner regions of galaxies may be similar to massive galaxies with respect to their metallicities. By using the $M_{\rm stellar}$ as a different approach, we suspect metallicity may be a potential variable in making high-$v_{\rm Si\,II}$ SNe Ia different from normal-$v_{\rm Si\,II}$ SNe Ia. This is also supported by the evidence that high-$v_{\rm Si\,II}$ SNe Ia appear to be redder than normal-$v_{\rm Si\,II}$ SNe Ia (Foley & Kasen 2011), together with recent observational results that SNe Ia in metal-rich environments are redder than those in metal-poor environments (Childress et al. 2013a; Pan et al. 2014).

Lentz et al. (2000) showed that the C+O layer metallicity in SN Ia explosion could play a role in affecting the observed Si II λ6355 velocity. The blue-shifted velocities of the silicon features increase with C+O layer metallicity due to the increasing opacity in the C+O layer moving the features blueward and causing larger line velocities. We determined a linear relation between the Si II λ6355 velocity and C+O metallicity of SN progenitor using the models of Lentz et al. (2000). The Si II λ6355 velocities were measured from their SN Ia model spectra using the same technique described in Section 3. The result shows the Si II λ6355 velocities increase with metallicities with a slope of $\sim$435 km s^{-1} dex^{-1}.

We determined the trend between Si II λ6355 velocity and metallicity using our sample by converting our host $M_{\rm stellar}$ to gas-phase metallicity in Fig. 4. The mass–metallicity relation studied from Kewley & Ellison (2008) was used for the conversion. We found the Si II λ6355 velocities increase with metallicity with a slope of $\sim$1357 km s^{-1} dex^{-1}. The slope determined from our data is in qualitative agreement with that of Lentz et al. (2000) models, although ours shows a steeper trend. The number of direct metallicity measurements from host spectroscopic data in this work do not allow for a sufficient statistical power to reveal if metallicity is important factor in altering the $v_{\rm Si\,II}$. However, given the tight relation between $M_{\rm stellar}$ and metallicity, this does offer a possible explanation that high-$v_{\rm Si\,II}$ SNe Ia could originate from more metal-rich populations than normal-$v_{\rm Si\,II}$ SNe Ia.

5.2 The physical origin of HVFs

In this work, we found SNe Ia with strong Ca II NIR HVFs present different properties to those with weaker HVFs. The physical origin of HVFs in SNe Ia is not yet clear. They are common in SN Ia spectra, and many scenarios have been proposed by previous studies (Wang et al. 2003; Gerardy et al. 2004; Mazzali et al. 2005a,b; Quimby et al. 2006; Tanaka et al. 2006, 2008; Childress et al. 2013b, 2014). Briefly speaking, the HVFs could be produced by either an abundance enhancement or a density enhancement. An abundance enhancement could be caused by an enhancement of intermediate-mass elements (IMEs) in the outer regions of the SN ejecta. A mixing with hydrogen from circumstellar material (CSM) could also increase the electron density and strengthen the recombination, which will result in a stronger Ca II feature. A density enhancement could result from the SN explosion itself, or the interaction between SN ejecta and CSM – or both .

We have confirmed that SNe Ia with a large R$_{\rm HVF}$ are higher stretch (and therefore brighter) than those with a small R$_{\rm HVF}$. We found a strong trend that they are found in galaxies with a lower stellar mass and a stronger sSFR. Maguire et al. (2014) show that although this relation is partially driven by higher-stretch SNe Ia having weaker photospheric Ca II NIR, this does not explain the entire trend; higher stretch SNe Ia also have stronger HVFs.

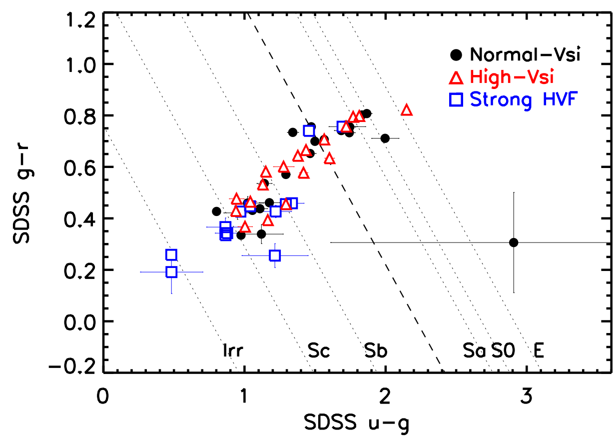

Figure 14. The rest-frame SDSS $g-r$ versus $u-g$ host galaxy colour for our SN Ia sample. The empirical relation studied by Strateva et al. (2001) is used to type the host galaxies. The dotted lines show the average $u-r$ for Irr(0.76), Sc(1.29), Sb(1.74), Sa(2.56), S0(2.68) and E(2.91) galaxies and the dashed line is the criterion to separate the late-type (left) and early-type (right) galaxies. The normal-$v_{\rm Si\,II}$ SNe Ia, high-$v_{\rm Si\,II}$ SNe Ia and SNe Ia with strong HVFs are shown in solid circles, open triangles and open squares, respectively.

In Fig. 14 we plot the rest-frame colour-colour diagram (SDSS $g-r$ against $u-g$) of our host galaxies. Following the procedure described in Lamareille et al. (2006), we further classify our host galaxies into different Hubble types based on the criteria proposed by Strateva et al. (2001). The mean $u-r$ values for six different spectral types of galaxies are overplotted. Although the $u-r$ values used here have some uncertainty due to dust extinction in the galaxy, overall it provides a good idea of the Hubble types of our hosts.

The host galaxies of SNe Ia with a large R$_{\rm HVF}$ concentrate toward the blue end of the host galaxy colour sequence. These galaxies are mostly classified as Sb/Sc/Irr galaxies, whereas the high-$v_{\rm Si\,II}$ SNe Ia are found in both late-type and early-type galaxies. This is consistent with Section 4.2, where we showed that SNe Ia with HVFs arise in galaxies with very strong sSFRs, and are therefore likely to be related to young stellar populations. This argues against an orientation or viewing angle effect (confirming the results of Tanaka et al. 2006) being purely responsible for the presence of HVFs in SN Ia spectra, as there is no reason that the orientation would depend on the underlying stellar population.

Using narrow blue-shifted Na I D absorption features as a probe of this CSM, Sternberg et al. (2011) and Maguire et al. (2013) found an excess of SNe Ia with blueshifted narrow Na I D features, showing CSM around their progenitors. They further found the host galaxies of these SNe Ia are mostly late-type galaxies. If the HVFs observed in SN spectra are related to the interaction between the SN ejecta and a CSM, our work is consistent with Maguire et al.: SNe Ia presenting strong HVFs tend to explode in galaxies with young stellar populations. This provides further evidence for at least two different populations of SNe Ia (see discussion in Maguire et al. 2013), given the distinct properties of host galaxies between SNe Ia with strong HVFs and weak HVFs/high-$v_{\rm Si\,II}$ SNe Ia. In Table 3 we summarise the prop-

Table 3. The comparison between normal-$v_{\rm Si\,II}$/weak HVFs SNe Ia, high-$v_{\rm Si\,II}$ SNe Ia and SNe Ia with strong HVFs.

	Normal $v_{\rm Si\,II}$ & weak HVFs	High $v_{\rm Si\,II}$	Strong HVFs
SN stretch	$0.6 < s < 1.1$	$0.8 < s < 1.1$	$s > 1.0$
$v_{\rm Si\,II}$	–	–	< 12000 km s^{-1}
Host type	E to Sc	E to Sc	Sb/Sc/Irr
Host $M_{\rm stellar}$	low mass/massive	massive	prefer low mass
Host sSFR	low/intermediate	intermediate	high

erties of high-$v_{\rm Si\,II}$ SNe Ia and SNe Ia with strong HVFs found in this work.

6 CONCLUSIONS

In this paper we have analysed spectroscopic measurements of 122 type Ia supernovae (SNe Ia) with $z < 0.09$ discovered by the Palomar Transient Factory. In particular, we focused on the velocity and pseudo equivalent widths of the Si II λ6355 and Ca II near-infrared triplet (NIR) absorptions. We determined the host parameters using both photometric and spectroscopic data, and estimated the host $M_{\rm stellar}$, SN–host offset, star formation rate (SFR), metallicity and age. Various relations between SN spectral features and host parameters are demonstrated in this work. Below we summarise our main findings.

- We find that SNe Ia with a high-Si II λ6355 velocity (high-$v_{\rm Si\,II}$) are preferentially found in massive host galaxies, whereas SNe Ia with normal-$v_{\rm Si\,II}$ are found in hosts of all stellar mass (Fig. 4). We find weaker, but consistent, trends when considering the Ca II NIR feature in place of Si II λ6355.
- There is also some evidence that these high-$v_{\rm Si\,II}$ SNe Ia are found in the inner regions of their host galaxies (Fig. 7). However, this trend is not as statistically significant in our sample as in previous studies.
- If stellar mass is intepreted as a proxy for metallicity, and inner regions of galaxies are more metal rich, these findings are consistent with a metallicity dependence in $v_{\rm Si\,II}$. Such a qualitative dependence is seen in some models of SN Ia spectra.
- SNe Ia with a strong R$_{\rm HVF}$ (defined as the ratio of the pEWs of the high-velocity and photospheric components of the Ca II near-IR feature) are preferentially found in galaxies with a lower stellar mass, a bluer colour and a stronger sSFR (Figs. 12 and 13). Their host SEDs are consistent with being of morphological type Sc and later (Fig. 14).
- This strongly suggests that SNe Ia with a large R$_{\rm HVF}$ originate from young stellar populations, and argues against an orientation effect being purely responsible for HVFs in SNe Ia. Previous studies proposed a strong link between SN Ia HVFs and circumstellar material (CSM), and found most of the SNe Ia showing signatures of CSM explode in late-type galaxies. Our results are consistent with these findings, assuming that the HVFs are related to the interaction between the SN ejecta and a CSM local to the SN.

Investigating the relationships between SN spectral features and host galaxy parameters provides a different angle to probe the nature of the SN explosion. Host studies have been proven to be useful in previous works, especially in the relations with SN luminosities. Here in this work we show there is also a strong connection between SN Ia spectral features and their host galaxies, which is worth further investigation and study.

ACKNOWLEDGEMENTS

MS acknowledges support from the Royal Society and EU/FP7-ERC grant no [615929]. A.G.-Y. is supported by the EU/FP7-ERC grant no [307260], the Quantum Universe I-Core program by the Israeli Committee for planning and funding and the ISF, GIF, Minerva and ISF grants, and Kimmel and ARCHES awards. This research used resources of the National Energy Research Scientific Computing Center, which is supported by the Office of Science of the U.S. Department of Energy under Contract No. DE-AC02-05CH11231. Observations obtained with the Samuel Oschin Telescope at the Palomar Observatory as part of the Palomar Transient Factory project, a scientific collaboration between the California Institute of Technology, Columbia University, Las Cumbres Observatory, the Lawrence Berkeley National Laboratory, the National Energy Research Scientific Computing Center, the University of Oxford, and the Weizmann Institute of Science. The William Herschel Telescope is operated on the island of La Palma by the Isaac Newton Group in the Spanish Observatorio del Roque de los Muchachos of the Instituto de Astrofisica de Canarias. Based on observations obtained at the Gemini Observatory, which is operated by the Association of Universities for Research in Astronomy, Inc., under a cooperative agreement with the NSF on behalf of the Gemini partnership: the National Science Foundation (United States), the National Research Council (Canada), CONICYT (Chile), the Australian Research Council (Australia), Ministério da Ciência, Tecnologia e Inovação (Brazil) and Ministerio de Ciencia, Tecnología e Innovación Productiva (Argentina). Based on Gemini programs GN-2010B-Q-111, GS-2010B-Q-82, GN-2011A-Q-82, GN-2011B-Q-108, GN-2012A-Q-91, GS-2012A-Q-3, GN-2012B-Q-122, and GS-2012B-Q-83 for the host galaxy observations, and GN-2010A-Q-20, GN-2010B-Q-13, GN-2011A-Q-16 and GS-2009B-Q-11 for the SN observations. This work makes use of observations from the LCOGT network. Some of the data presented herein were obtained at the W.M. Keck Observatory, which is operated as a scientific partnership among the California Institute of Technology, the University of California and the National Aeronautics and Space Administration. The Observatory was made possible by the generous financial support of the W.M. Keck Foundation. Based on observations collected at the European Organisation for Astronomical Research in the Southern Hemisphere, Chile, under program IDs 084.A-

0149 and 085.A-0777. Observations obtained with the SuperNova Integral Field Spectrograph on the University of Hawaii 2.2-m telescope as part of the Nearby Supernova Factory II project, a scientific collaboration between the Centre de Recherche Astronomique de Lyon, Institut de Physique Nucl'eaire de Lyon, Laboratoire de Physique Nucl'eaire et des Hautes Energies, Lawrence Berkeley National Laboratory, Yale University, University of Bonn, Max Planck Institute for Astrophysics, Tsinghua Center for Astrophysics, and Centre de Physique des Particules de Marseille.

This research has made use of the NASA/IPAC Extragalactic Database (NED) which is operated by the Jet Propulsion Laboratory, California Institute of Technology, under contract with the National Aeronautics and Space Administration.

This publication has been made possible by the participation of more than 10 000 volunteers in the Galaxy Zoo: Supernovae project (`http://supernova.galaxyzoo.org/authors`).

REFERENCES

Ahn C. P. et al., 2013, ArXiv e-prints
Bailey S. J. et al., 2009, in Bulletin of the American Astronomical Society, Vol. 41, American Astronomical Society Meeting Abstracts #213, p. 321.05
Baldwin J. A., Phillips M. M., Terlevich R., 1981, PASP, 93, 5
Benetti S. et al., 2005, ApJ, 623, 1011
Bertin E., Arnouts S., 1996, A&AS, 117, 393
Betoule M. et al., 2014, ArXiv e-prints
Blondin S., Mandel K. S., Kirshner R. P., 2011, A&A, 526, A81
Blondin S. et al., 2012, AJ, 143, 126
Bloom J. S. et al., 2012a, ApJ, 744, L17
Bloom J. S. et al., 2012b, PASP, 124, 1175
Branch D. et al., 2006, PASP, 118, 560
Branch D., van den Bergh S., 1993, AJ, 105, 2231
Brown T. M. et al., 2013, ArXiv e-prints
Cappellari M., Emsellem E., 2004, PASP, 116, 138
Childress M. et al., 2013a, ApJ, 770, 108
Childress M. J., Filippenko A. V., Ganeshalingam M., Schmidt B. P., 2014, MNRAS, 437, 338
Childress M. J. et al., 2013b, ApJ, 770, 29
Conley A. et al., 2008, ApJ, 681, 482
D'Andrea C. B. et al., 2011, ApJ, 743, 172
Dilday B. et al., 2012, Science, 337, 942
Faber S. M. et al., 2003, in Society of Photo-Optical Instrumentation Engineers (SPIE) Conference Series, Vol. 4841, Instrument Design and Performance for Optical/Infrared Ground-based Telescopes, Iye M., Moorwood A. F. M., eds., pp. 1657–1669
Foley R. J., 2012, ApJ, 748, 127
Foley R. J., 2013, MNRAS, 435, 273
Foley R. J., Kasen D., 2011, ApJ, 729, 55
Foley R. J. et al., 2012, ApJ, 752, 101
Galbany L. et al., 2012, ApJ, 755, 125
Gallagher J. S., Garnavich P. M., Berlind P., Challis P., Jha S., Kirshner R. P., 2005, ApJ, 634, 210
Gallagher J. S., Garnavich P. M., Caldwell N., Kirshner R. P., Jha S. W., Li W., Ganeshalingam M., Filippenko A. V., 2008, ApJ, 685, 752
Gerardy C. L. et al., 2004, ApJ, 607, 391
Hachinger S., Mazzali P. A., Benetti S., 2006, MNRAS, 370, 299
Hakobyan A. A., Mamon G. A., Petrosian A. R., Kunth D., Turatto M., 2009, A&A, 508, 1259
Hamuy M., Phillips M. M., Suntzeff N. B., Schommer R. A., Maza J., Aviles R., 1996, AJ, 112, 2391
Hamuy M., Trager S. C., Pinto P. A., Phillips M. M., Schommer R. A., Ivanov V., Suntzeff N. B., 2000, AJ, 120, 1479
Hayden B. T., Gupta R. R., Garnavich P. M., Mannucci F., Nichol R. C., Sako M., 2013, ApJ, 764, 191
Henry R. B. C., Worthey G., 1999, PASP, 111, 919
Hook I. M., Jørgensen I., Allington-Smith J. R., Davies R. L., Metcalfe N., Murowinski R. G., Crampton D., 2004, PASP, 116, 425
Iben, Jr. I., Tutukov A. V., 1984, ApJS, 54, 335
Johansson J. et al., 2013, MNRAS, 435, 1680
Kelly B. C., 2007, ApJ, 665, 1489
Kelly P. L., Hicken M., Burke D. L., Mandel K. S., Kirshner R. P., 2010, ApJ, 715, 743
Kennicutt J. R. C., 1998, ARA&A, 36, 189
Kessler R. et al., 2009, ApJS, 185, 32
Kewley L. J., Dopita M. A., Sutherland R. S., Heisler C. A., Trevena J., 2001, ApJ, 556, 121
Kewley L. J., Ellison S. L., 2008, ApJ, 681, 1183
Lamareille F., Contini T., Le Borgne J.-F., Brinchmann J., Charlot S., Richard J., 2006, A&A, 448, 893
Lampeitl H. et al., 2010, ApJ, 722, 566
Lantz B. et al., 2004, in Society of Photo-Optical Instrumentation Engineers (SPIE) Conference Series, Vol. 5249, Optical Design and Engineering, Mazuray L., Rogers P. J., Wartmann R., eds., pp. 146–155
Law N. M. et al., 2009, PASP, 121, 1395
Le Borgne D., Rocca-Volmerange B., 2002, A&A, 386, 446
Lentz E. J., Baron E., Branch D., Hauschildt P. H., Nugent P. E., 2000, ApJ, 530, 966
Maguire K. et al., 2012, MNRAS, 426, 2359
Maguire K. et al., 2014, MNRAS, 444, 3258
Maguire K. et al., 2013, MNRAS, 436, 222
Mannucci F., Della Valle M., Panagia N., Cappellaro E., Cresci G., Maiolino R., Petrosian A., Turatto M., 2005, A&A, 433, 807
Maoz D., Mannucci F., Nelemans G., 2013, ArXiv e-prints
Marion G. H. et al., 2013, ApJ, 777, 40
Markwardt C. B., 2009, in Astronomical Society of the Pacific Conference Series, Vol. 411, Astronomical Data Analysis Software and Systems XVIII, Bohlender D. A., Durand D., Dowler P., eds., p. 251
Mazzali P. A. et al., 2005a, ApJ, 623, L37
Mazzali P. A., Benetti S., Stehle M., Branch D., Deng J., Maeda K., Nomoto K., Hamuy M., 2005b, MNRAS, 357, 200
Mazzali P. A., Röpke F. K., Benetti S., Hillebrandt W., 2007, Science, 315, 825
Miller J. S., Stone R. P. S., 1993, Lick Obs. Tech. Rep., No. 66
Nugent P., Phillips M., Baron E., Branch D., Hauschildt P., 1995, ApJ, 455, L147

Nugent P. E. et al., 2011, Nature, 480, 344
Oke J. B. et al., 1995, PASP, 107, 375
Oke J. B., Gunn J. E., 1982, PASP, 94, 586
Pan Y.-C. et al., 2014, MNRAS, 438, 1391
Patat F., Baade D., Höflich P., Maund J. R., Wang L., Wheeler J. C., 2009, A&A, 508, 229
Perlmutter S. et al., 1999, ApJ, 517, 565
Pettini M., Pagel B. E. J., 2004, MNRAS, 348, L59
Quimby R., Höflich P., Kannappan S. J., Rykoff E., Rujopakarn W., Akerlof C. W., Gerardy C. L., Wheeler J. C., 2006, ApJ, 636, 400
Rahmer G., Smith R., Velur V., Hale D., Law N., Bui K., Petrie H., Dekany R., 2008, in Society of Photo-Optical Instrumentation Engineers (SPIE) Conference Series, Vol. 7014, Society of Photo-Optical Instrumentation Engineers (SPIE) Conference Series
Rau A. et al., 2009, PASP, 121, 1334
Rest A. et al., 2013, ArXiv e-prints
Riess A. G. et al., 1998, AJ, 116, 1009
Riess A. G. et al., 2007, ApJ, 659, 98
Rigault M. et al., 2013, A&A, 560, A66
Salpeter E. E., 1955, ApJ, 121, 161
Sánchez-Blázquez P. et al., 2006, MNRAS, 371, 703
Sarzi M. et al., 2006, MNRAS, 366, 1151
Schaefer B. E., Pagnotta A., 2012, Nature, 481, 164
Silverman J. M., Ganeshalingam M., Li W., Filippenko A. V., 2012a, MNRAS, 425, 1889
Silverman J. M., Kong J. J., Filippenko A. V., 2012b, MNRAS, 425, 1819
Smith A. M. et al., 2011, MNRAS, 412, 1309
Steele I. A. et al., 2004, in Society of Photo-Optical Instrumentation Engineers (SPIE) Conference Series, Vol. 5489, Society of Photo-Optical Instrumentation Engineers (SPIE) Conference Series, Oschmann Jr. J. M., ed., pp. 679–692
Sternberg A. et al., 2011, Science, 333, 856
Strateva I. et al., 2001, AJ, 122, 1861
Sullivan M. et al., 2010, MNRAS, 406, 782
Sullivan M. et al., 2006, ApJ, 648, 868
Sullivan M., et al., 2011, ApJ, 737, 102
Tanaka M. et al., 2008, ApJ, 677, 448
Tanaka M., Mazzali P. A., Maeda K., Nomoto K., 2006, ApJ, 645, 470
Tremonti C. A. et al., 2004, ApJ, 613, 898
Vazdekis A., Sánchez-Blázquez P., Falcón-Barroso J., Cenarro A. J., Beasley M. A., Cardiel N., Gorgas J., Peletier R. F., 2010, MNRAS, 404, 1639
Vernet J. et al., 2011, A&A, 536, A105
Wang L. et al., 2003, ApJ, 591, 1110
Wang X. et al., 2009, ApJ, 699, L139
Wang X., Wang L., Filippenko A. V., Zhang T., Zhao X., 2013, Science, 340, 170
Webbink R. F., 1984, ApJ, 277, 355
Whelan J., Iben, Jr. I., 1973, ApJ, 186, 1007
Yaron O., Gal-Yam A., 2012, PASP, 124, 668